Uncovering Molecular Mechanisms of Electrowetting and Saturation with Simulations

Jin Liu, Moran Wang, Shiyi Chen, and Mark O. Robbins

Phys. Rev. Lett. **108**, 216101 — Published 21 May 2012

DOI: 10.1103/PhysRevLett.108.216101

Uncovering Molecular Mechanisms of Electrowetting and Saturation with Simulations

Jin Liu[1], Moran Wang[1,2], Shiyi Chen[1,3] and Mark O. Robbins[1,4*]
[1]*Department of Mechanical Engineering, Johns Hopkins University, Baltimore, MD 21218, USA*
[2]*School of Aerospace, Tsinghua University, Beijing 100084, China*
[3]*State Key Laboratory for Turbulence and Complex Systems and CAPT College of Engineering, Peking University, China and*
[4]*Department of Physics and Astronomy, Johns Hopkins University, Baltimore, MD 21218, USA*

Molecular dynamics simulations are used to explore the physical mechanisms of electrowetting and the limits of continuum theories. Nanoscale drops exhibit the same behavior seen in macroscopic experiments: The contact angle θ follows continuum theory at low voltages and then saturates. Saturation limits applications of electrowetting and its origin is of great interest. In the simulations, saturation occurs when ions are pulled from the drop by large local fields. Saturation can be controlled by changing temperature, screening or the energy binding ions to the fluid. We show a local force balance equation for θ remains valid even after saturation and that the interface approaches the equilibrium contact angle within a few nanometers of the solid.

In electrowetting, an applied voltage V changes the macroscopic contact angle θ of a liquid drop on a solid. While electrowetting has proved useful in manipulating small drops [1–6], applications are limited because θ always saturates as V increases. The cause of saturation and the physics underlying electrowetting have been the subject of active debate [6–14], and previous theories have been limited to continuum models that become inadequate as drops shrink to micro or nanometer scales.

In this letter, we use molecular simulations to explore the atomistic underpinnings of electrowetting and the limits of continuum theory. Nanoscale drops exhibit the same behavior seen in macroscopic experiments. Initially, the decrease in contact angle with increasing V follows continuum theory, but θ saturates at large V. Saturation occurs when charged molecules are pulled from the drop and is controlled by local electric field strengths and molecular binding. An alternative expression for θ based on local force balance remains valid even after saturation and explains why θ approaches the equilibrium contact angle within a few nanometers of the solid. This is also the typical scale of atomistic effects.

The basic process of electrowetting on dielectric (EWOD), and the geometry of our simulations, are illustrated in Fig. 1(a). A dielectric layer of thickness D separates a conducting fluid drop and an electrode. As the voltage between drop and electrode increases, the drop spreads to lower the electrostatic energy. The associated decrease in macroscopic contact angle $\theta(V)$ is predicted to follow the Young-Lippmann equation (YLE) [15, 16]

$$\cos\theta(V) = \cos\theta_0 + cV^2/2\gamma, \qquad (1)$$

where θ_0 is the equilibrium contact angle at zero voltage, c the capacitance per unit area and γ the liquid-vapor surface tension. For the usual case of a dielectric that is thinner than the drop diameter, $c = \epsilon/D$, where ϵ is the permittivity.

Experiments have observed electrowetting with a wide range of fluids and substrates [17]. In all cases, results follow the YLE at small V, but saturate before perfect wetting is achieved. Indeed, it is difficult to find systems where θ can be reduced from above 90^o to below 45^o. A variety of mechanisms for saturation have been proposed [7–14], but no consensus has emerged for its origin.

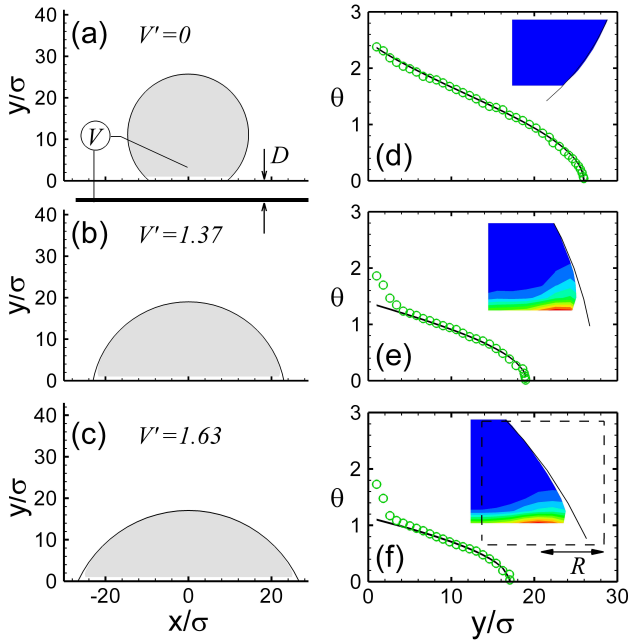

FIG. 1. (a-c) As the voltage between a cylindrical drop and electrode (thick line) increases, the drop (shaded) spreads along a dielectric of thickness $D = 4.85\sigma$. Solid lines show cylindrical fits to the drop surface for $y > 6\sigma$. (d-f) Angle of drop surface vs. height (points) and cylindrical fit (line). The angle approaches θ_0 near the solid, as shown in the inset plots, where colors from blue to red also indicate increasing charge density. A box of edge $2R = 8\sigma$ in (f) indicates the volume used to define the force balance in Eq. 2. Chains have 4 beads, $\theta_0 = 138^o$, and $l_B = 4.0\sigma$.

One mechanism is based on the electrocapillary model for the YLE. The equilibrium contact angle $\cos\theta_0 = (\gamma_{vs} - \gamma_{ls})/\gamma$, where γ_{ls} and γ_{vs} are the liquid-solid and

vapor-solid tensions. The YLE follows from the same relation if the electrostatic energy per area in the dielectric is incorporated into an effective liquid-solid tension, $\gamma_{ls} - cV^2/2$. Ralston and coworkers have found that saturation often occurs when this effective tension becomes negative, indicating an instability [10, 12]. However, there is ambiguity in the values of γ_{ls} and γ_{vs} which are not measured directly[6], and recent measurements of thin films show no change in the solid-liquid tension [18].

The YLE can also be derived from an electromechanical view, using the local balance of capillary and electrostatic forces along the interface [19–21]. A detailed theoretical analysis [19] shows the interface angle fits Eq. 1 at large scales and approaches θ_0 near the solid. Experiments at mm scales support these calculations of the drop shape [18, 21], but the theory does not provide an explanation for saturation. This may reflect the approximations that are made. In particular, the fluid is treated as a perfect conductor and D is the only length scale in the model. The screening length, interfacial width and other length scales become important as drop dimensions decrease. Molecular dynamics simulations can determine the role of these length scales and provide direct tests of assumptions in the electrocapillary and electromechanical interpretations. Previous simulations have provided insight into electrocapillary effects [22, 23], but have not examined EWOD.

Given the universal nature of the effects observed in electrowetting, we use a generic molecular model that has been useful in fundamental studies of wetting [24, 25]. The fluid consists of short chains of n spheres bound by covalent bonds modeled with a FENE potential [26]. Intermolecular interactions are modeled with a truncated Lennard-Jones (LJ) potential with binding energy u, molecular diameter σ, and cutoff distance $r_c = 2.5\sigma$. The substrate is the (111) surface of a rigid fcc crystal with nearest-neighbor spacing 1.32 σ. The binding energy u' of the LJ potential between fluid and solid was varied to change θ_0 [27]. A Langevin thermostat maintained a constant temperature T above the glass temperature $T_g \sim 0.5u/k_B$, where k_B is Boltzmann's constant [28].

Long-range Coulomb interactions between charges were treated using a highly efficient and accurate multigrid Particle-Particle Particle-Mesh algorithm [29]. Given the difficulty in accurately representing the molecular level changes in ϵ near solid and liquid surfaces, we used a uniform ϵ. Dielectric contrast will change the spatial distribution of fringing fields, but as shown below, this does not affect the saturation mechanism. To model an electrode, we introduced image charges that enforced a constant voltage at a depth D below the solid surface (Fig. 1(a)). Values of c and γ were determined from simulations with a fluid film of uniform thickness [30] and were nearly independent of V.

As noted above, several length scales that do not enter previous continuum treatments may become important at the nanoscale. Two structural lengths are the molecular diameter $\sigma \sim 0.5$nm and the full width ξ of the fluid interface. In most cases the two are of the same order, and in our simulations $\xi \sim 3\sigma$. The strength of dielectric screening can be characterized by the Bjerrum length $l_B = e^2/\epsilon k_B T$, at which Coulomb interactions equal the thermal energy. Increasing ϵ reduces both the Bjerrum length and the effective strength of Coulomb interactions. Another scale is the screening length λ for charge near the solid wall. In our simulations, atomistic effects are important and $\lambda \sim 2 - 4\sigma$ (Fig. 1(d-f)) [29].

We studied a wide range of systems and found all gave behavior similar to that shown in the figures. The temperature was varied from $k_B T/u = 0.6$ to 0.9, with results for 0.7 shown below. The ratio of fluid interactions with fluid and solid, u'/u, was changed from 0.4 to 0.6 ($\theta_0 = 138^\circ$ and 114°). Results for $D = 4.86\sigma$ ($c = 0.19\epsilon/\sigma$) are shown but similar results are found for $D/\sigma = 1.62$ to 15.67. Chain length was varied from 4 to 8 ($\gamma\sigma^2/u = 1.08$ and 1.17). The dielectric constant was varied by more than an order of magnitude, changing l_B/σ from 4 to 96.

Simulations of electrowetting used a cylindrical drop geometry to eliminate line tension effects [16, 27], and results are averaged along the cylinder's axis, z. Periodic boundary conditions were applied in all three directions. The period along z, 10.6 σ, was small enough to prevent the pearling instability [16]. Long periods were used along x and y (116 σ and 51.8 σ) and forces from periodic images were removed using the correction in Ref. [31]. Heights are measured from the top layer of solid atoms. Results were averaged over four independent simulations with 6192 beads. Consistent results were obtained when the number of beads was tripled and/or system dimensions doubled.

The voltage is changed by adding an electron charge e to one sphere on a given number of chains and equilibrating for at least 3000τ, where $\tau = \sqrt{m\sigma^2/u}$ is the characteristic LJ time. Results were then averaged for a further 3000τ. To ensure there was sufficient time for equilibration, results for increasing and deceasing V were compared. No difference was seen before saturation within the statistical errorbars. These are smaller than the symbol size in the figures.

Figure 1 shows how the drop shape changes with V, as well as the distribution of charge. The interface was defined as the surface where the density was half the bulk value. Since $\theta(V)$ represents the macroscopic angle far from the solid, it was obtained by extrapolating cylindrical fits to the interface for $y > 6\sigma$ down to $y = 0$.

Figure 2(a) shows $\theta(V)$ for a wide range of parameters. In each case, the results follow Eq. 1 at low V and then saturate. Since c and γ were obtained from independent simulations, there are no adjustable parameters. These results provide strong evidence that the YLE remains valid down to nanometer scales.

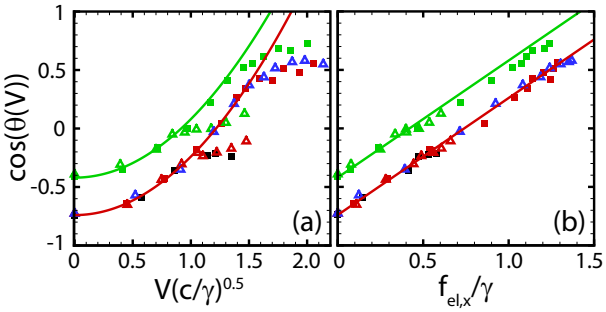

FIG. 2. (a) Change in contact angle θ with dimensionless voltage (points) and prediction of Eq. 1 (lines). Upper results (green) are for $\theta_0 = 114^o$ and lower are for $\theta_0 = 138^o$. Squares and triangles are for chains with 8 and 4 beads, respectively. For most data $l_B = 12.32\sigma$. Blue triangles and black squares show results for $l_B = 4.0\sigma$ (stronger screening) and $l_B = 96.08\sigma$ (weaker screening), respectively. (b) Same results plotted against $f_{el,x}$ and the predictions of Eq. 2 (lines).

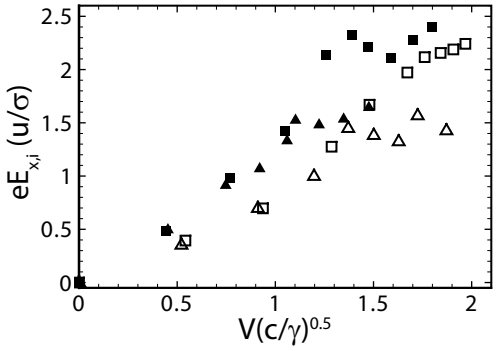

FIG. 3. Variation of the electric force at the interface, $eE_{x,i}$, with V for $\theta_0 = 138^o$. Squares and triangles are for chains with 8 and 4 beads, respectively. Closed and open symbols are for $l_B = 12.32\sigma$ and $l_B = 4.0\sigma$, respectively.

The voltage at saturation V_{sat} varies dramatically, increasing with increasing chain length and decreasing l_B (weaker Coulomb interactions). These results are clearly inconsistent with the electrocapillary model for saturation. First the interfacial tensions (and hence θ_0 in Fig. 2) are nearly independent of chain length. Moreover, since the solid is rigid, both γ_{ls} and γ_{vs} can be viewed as much larger than γ so the electrocapillary model predicts no saturation. Direct evaluation of the *local* interfacial tensions shows little variation with V, as concluded from recent experiments [18]. Finally, the saturation angle is independent of l_B in the electrocapillary model.

Direct observation of molecular configurations in our simulations shows that saturation is associated with individual charged molecules being pulled from the drop by large local electric fields $\vec{E}$. This lowers the electrostatic energy in much the same way as spreading of the entire drop. The escaped molecules screen $\vec{E}$ near the contact line, limiting the number of molecules that escape.

Figure 3 shows the peak electric force on molecules at the interface, $eE_{x,i}$, for a range of systems. The peak was always in the lowest layer of the fluid. For all systems, $eE_{x,i}$ rises linearly at small V and then saturates. The linear rise depends on the factors that determine $\theta(V)$ (D, c, ϵ and γ), but is independent of chain length. In contrast, for these and other simulations parameters, values of $eE_{x,i}$ for a given chain length saturate at the same force. Each time V is increased beyond saturation, the local field starts to increase. However, the larger force pulls more molecules from the drop, bringing $eE_{x,i}$ back towards the saturation value. Small fluctuations are present in $eE_{x,i}$ because of the small size of the drop and the discreteness of charges.

Increasing l_B (stronger Coulomb interactions), makes $eE_{x,i}$ rise more rapidly with V and lowers V_{sat}. Increasing l_B also increases the volume where the field is large, but this increase in volume does not directly affect the value of $eE_{x,i}$ at saturation. The value of V_{sat} depends only weakly on θ_0 which has a small effect on the peak field. Increasing chain length increases the energy barrier for removing molecules and thus both $eE_{x,i}$ and V_{sat}. Both the force and V_{sat} decreased with increasing T.

Other authors have suggested different ways that changes in charge distribution could lead to saturation. One proposed mechanism is similar to ours, but involves ejection of charged droplets rather than individual molecules [7]. Another finds an instability to radial deformations [13]. Saturation in both models depends on surface tension, and thus would not predict the variation with chain length observed here. Verheijen and Prins [8] considered a model where dielectric breakdown led to a layer of bound charge at some distance below the fluid. This reduces the force driving a decrease in contact angle by a constant amount rather than causing saturation at a constant value. Note that this type of charge trapping does not happen in our simulations and that there is also no charge transport through the dielectric as assumed in Ref. [11]. Finally, Ref. [14] finds that the impedance of a counterelectrode can produce saturation at high frequencies, but our simulations are for dc and have no electrode.

Further insight into the mechanisms of electrowetting and the origin of saturation is provided by extending the electromechanical concept of local force balance [20, 21] down to nanometer scales. The finite width of the interface and the screening length cannot be ignored, but one can consider force balance on a volume of width $2R$ (Fig. 1(f)) enclosing the contact line. The only net forces are the integrated electrostatic force per unit length $f_{el,x}$ on the internal charge density and the capillary forces from the interfaces leaving the volume. As long as $2R > \xi$, the integrated capillary force can be represented by the interfacial tension directed along the tangent direction[30].

Force balance along the solid surface requires:

$$\gamma_{vs} - \gamma_{ls} - \gamma\cos(\theta_R) + f_{el,x} = 0, \quad (2)$$

where θ_R is the angle of the drop at the edge of the volume. Note that $\theta_R = \theta_0$ if $f_{el,x} = 0$. From direct measurements we found the interfacial tensions change little with V, so equilibrium values can be used in Eq. 2.

In our simulations, using $R = 4\sigma$ includes the entire electrostatic force [32]. Eq. 2 then gives $\theta_R \sim \theta(V)$, with small corrections from the curvature of the drop, and the associated change in θ with height. Figure 2(b) shows that measured values of $f_{el,x}$ and $\theta(V)$ are consistent with Eq. 2 even after saturation has occurred. This is not surprising, since forces must balance in a static system. Escaping charge decreases $df_{el,x}/dV$, and thus the rate of increase in $\cos\theta(V)$, but Eq. 2 remains valid. In contrast, the YLE makes assumptions about the integrity of the drop that break down after saturation. Equation 2 only reduces to the YLE if the fringe fields around the drop edges do not change with drop width [6]. In this case the change in energy with the position of the drop edge comes from the change in electrostatic energy stored in the central region of the dielectric [6, 8, 21] and $f_{el,x} = cV^2/2$. When the charge distribution at the edges changes, the YLE breaks down.

If R is decreased from 4σ to 0, $f_{el,x} \to 0$ and Eq. 2 implies θ_R must approach θ_0. This trend is clearly evident in Fig. 1(d-f), although θ_R remains slightly below θ_0. This is an atomistic effect reflecting a breakdown of the assumption that R is larger than the interfacial width.

Atomistic effects also change θ at larger scales. Buehrle et al. [19] assumed perfect conductivity so $\vec{E}$ is perfectly screened, charge is confined to an infinitely sharp drop surface, and D is the only length scale. Then numerical solutions showed θ approached θ_0 at $R < 0.1D$. The insets in Fig. 1(e,f) show clearly that the charge extends throughout the contact line region. The fringing electric fields penetrate over a comparable distance ($\sim 4\sigma$) and Eq. 2 implies that θ changes over this screening scale. The YLE will fail when the entire droplet becomes comparable to this screening scale or ξ. Even for larger drops the screening length plays an important role by cutting off the divergence in electric field that is predicted by continuum theory [6].

In summary, our simulations of EWOD show that nanoscale drops exhibit the same behavior found in macroscopic experiments. The contact angle follows the continuum YLE at low voltages and saturates at high V. A generalization of the electromechanical view of EWOD to nanoscales leads to a force balance equation for θ that remains valid even after saturation. The analysis also shows that the contact angle must approach θ_0 near the solid. This conclusion is similar to mm scale studies [19, 21] where D is the only length scale. In nanoscale drops, atomistic effects cause the change in angle to be spread over scales that are comparable to the interface width and screening length.

The source of saturation is difficult to determine in experiments, but is clearly caused by molecules being pulled from the drop in our simulations. Saturation occurs when the peak electric force near the edge of the drop exceeds the molecular binding force. Increasing l_B (stronger Coulomb interactions), increases the peak force and promotes saturation. Increasing binding by increasing chain length or lowering temperature delays saturation.

This mechanism may explain the asymmetry in positive and negative values of V_{sat} observed in some experiments, since anions and cations will in general be bound with different strengths. There is some evidence [33] that larger molecules that interact over a greater surface area saturate at higher V, much like our longer chains. It is also interesting to note that larger values of $\cos(\theta)$ can be reached using ac voltages [6, 12], even though deviations from the YLE occur at comparable voltages. If the polarity changes fast enough, neither ion species will have time to escape far from the drop, reducing the screening from escaped molecules. It will be interesting to see if using fluids with higher molecular binding can delay saturation in experiments and improve EWOD performance.

We thank Shengfeng Cheng, Rohini Gupta, Patricia McGuiggan and Joelle Frechette for helpful discussions. This work was supported by the National Science Foundation (NSF) unders Grant CMS-0103408 and OCI-108849 and simulations were performed on the Homewood High Performance Cluster.

* mr@jhu.edu

[1] W. J. J. Welters and L. G. J. Fokkink, Langmuir **14**, 1535 (1998).
[2] M. G. Pollack, R. B. Fair, and A. D. Shenderov, Appl. Phys. Lett. **77**, 1725 (2000).
[3] B. Berge and J. Peseux, Eur. Phys. J. E **3**, 159 (2000).
[4] T. Krupenkin, S. Yang, and P. Mach, Appl. Phys. Lett. **82**, 316 (2003).
[5] R. A. Hayes and B. J. Feenstra, Nature **425**, 383 (2003).
[6] F. Mugele, Soft Matter **5**, 3377 (2009).
[7] M. Vallet, M. Vallade, and B. Berge, Eur. Phys. J. B **11**, 583 (1999).
[8] H. J. J. Verheijen and M. W. J. Prins, Langmuir **15**, 6616 (1999).
[9] B. Shapiro, H. Moon, R. L. Garrell, and C. J. Kim, J. Appl. Phys. **93**, 5794 (2003).
[10] A. Quinn, R. Sedev, and J. Ralston, J. Phys. Chem. B **109**, 6268 (2005).
[11] A. G. Papathanasiou, A. T. Papaioannou, and A. G. Boudouvis, J. Appl. Phys. **103**, 034901 (2008).
[12] M. Paneru, C. Priest, R. Sedev, and J. Ralston, J. Am. Chem. Soc. **132**, 8301 (2010).
[13] M. A. Fontelos and U. Kindelan, Q. J. Mech. Appl. Math **62**, 465 (2009).

[14] D. Klarman, D. Andelman, and M. Urbakh, Langmuir **27**, 6031 (2011).
[15] G. Lippmann, Ann. Chim. Phys. **5**, 494 (1875).
[16] P. G. D. Gennes, F. Brochard-Wyart, and D. Quere, *Capillarity and Wetting Phenomena: Drops, Bubbles, Pearls, Waves* (Springer, New York, 2003).
[17] F. Mugele and J. C. Baret, J. Phys.: Condens. Matter **17**, R705 (2005).
[18] R. Gupta, G. K. Olivier, and J. Frechette, Langmuir **26**, 11946 (2010).
[19] J. Buehrle, S. Herminghaus, and F. Mugele, Phys. Rev. Lett. **91**, 086101 (2003).
[20] T. Jones, J. Micromech. Microeng. **15**, 1184 (2005).
[21] F. Mugele and J. Buehrle, J. Phys.: Condens. Matter **19**, 375112 (2007).
[22] A. Kutana and K. P. Giapis, Nano Lett. **6**, 656 (2006).
[23] D. Bratko, C. D. Daub, K. Leung, and A. Luzar, J. Am. Chem. Soc. **129**, 2504 (2007).
[24] J. DeConinck, U. D'Ortona, J. Koplik, and J. R. Banavar, Phys. Rev. Lett. **74**, 928 (1995).
[25] P. A. Thompson and S. M. Troian, Nature **389**, 360 (1997).
[26] G. S. Grest and K. Kremer, Phys. Rev. A **33**, 3628 (1986).
[27] P. A. Thompson, W. B. Brinckerhoff, and M. O. Robbins, J. Adhesion Sci. Technol. **7**, 535 (1993).
[28] C. Bennemann, W. Paul, K. Binder, and B. Dünweg, Phys. Rev. E **57**, 843 (1998).
[29] J. Liu, M. Wang, S. Chen, and M. Robbins, J. Comput. Phys. **229**, 7834 (2010).
[30] J. G. Kirkwood and F. P. Buff, J. Chem. Phys. **17**, 338 (1949).
[31] I. Yeh and M. L. Berkowitz, J. Chem. Phys. **111**, 3155 (1999).
[32] For larger values of D, R must be increased as discussed below and in Ref. [19].
[33] B. Raj, M. Dhindsa, N. R. Smith, R. Laughlin, and J. Heikenfeld, Langmuir **25**, 12387 (2009).